

Charge transport in activated carbon electrodes: the behaviour of three electrolytes vis-à-vis their specific conductance

Pankaj¹ · Madhav P. Chavhan¹ · Somenath Ganguly¹

Received: 14 September 2016 / Revised: 23 February 2017 / Accepted: 23 February 2017 / Published online: 14 March 2017
© Springer-Verlag Berlin Heidelberg 2017

Abstract In this study, the electrochemical performances of different aqueous electrolytes (6 M KOH, 2 M KCl and 0.5 M K₂SO₄) in activated carbon electrodes are evaluated with regard to their use in electrochemical double layer capacitor (EDLC). The results from cyclic voltammetry, galvanostatic charge/discharge and electrochemical impedance spectroscopy (EIS) were analysed. The lowest value of equivalent series resistance (ESR) and the highest values of specific capacitance and coulombic efficiency were observed, when KOH was the electrolyte. The impedance spectroscopy plots were fitted to an equivalent circuit of ladder type to evaluate the resistances to ion transport at different levels of hierarchies in the pore network. Also, the quality of the double layer capacitance at lower hierarchy that primarily contributes to the overall capacitance of the device was evaluated from the leakage resistance in the equivalent circuit. The fitted circuit parameters were further reviewed vis-à-vis the specific conductance of chosen electrolyte, and the number of successive charge–discharge cycles prior to the EIS measurements.

Keywords Carbon · Supercapacitor · Electrolyte · Ion · Transport

Introduction

Electric double-layer capacitors (EDLCs), also known as supercapacitors have superior power density, reversibility

and long cycle life [1–4]. Supercapacitors bridge the gap between the electrolytic capacitors and batteries. These energy storage devices find applications, where peak power is required. In supercapacitors, the charge is stored electrostatically in a double layer on the surface of the electrode. Activated carbon (AC) is most widely used as electrode material due to its high specific surface area [3–13]. Most of the internal surface area of carbon material is contained in the lowest level of hierarchy in the pore network. Thus, the pore size distribution becomes equally important in charge transport.

Other than the internal pore structure of an electrode, the electrochemical performance of a supercapacitor depends on the electrochemical stability window, the size of electrolyte ions, the conductivity of the electrolyte and the choices of the electrode material and the current collector [5–12]. The ionic liquid based electrolytes provide widest electrochemical stability window (3–4 V), though its use is restricted due to high cost. Organic electrolytes offer a good stability window of 2.7–2.8 V at a less cost [2]. Aqueous electrolytes are inexpensive and environment friendly, while offering a narrower stability window. The acidic electrolytes have produced high capacitance, though its use is contingent upon sourcing a suitable anti-corrosive current collector [14]. Among alkaline electrolytes, 6 M KOH showed the highest ionic conductivity. Another aqueous electrolyte that has excellent stability is alkali sulphate. The stability window in this case exceeds 1.6 V, thus improving the energy density of the EDLC [14–14]. Also, the size of electrolyte ions with reference to the pore size may critically influence the electrochemical performance. The pores in the lowest hierarchy (i.e., the micro pores of size <2 nm) provide a significant fraction of the surface area for double layer capacitance. The access to these pores is required to achieve a high value of specific capacitance [11, 15–18]. Only the ions, smaller than the size of the micro pore can access the potential surface area to the fullest for charge storage [4, 18].

✉ Somenath Ganguly
snganguly@che.iitkgp.ernet.in

¹ Department of Chemical Engineering, Indian Institute of Technology, Kharagpur 721302, India

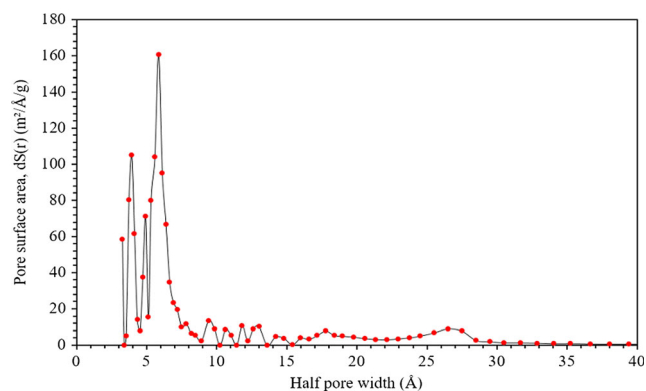


Fig. 1 DFT pore size distribution (activated carbon powder)

In this article, the electrochemical performance of 6 M KOH is compared with the performances of two neutral aqueous electrolytes. The cyclic voltammetry, galvanostatic charge/discharge and electrochemical impedance spectroscopy (EIS) studies were conducted for this purpose. Further, the impedance spectroscopy [19–27] results were analysed to understand the transport of ions in the pore network of activated carbon. The EIS results are fitted to an equivalent circuit of ladder type. The resistances, encountered by these electrolyte ions while penetrating into the multiple levels of hierarchy in the pore network are compared.

Methods

A slurry of carbon powder was prepared by mixing activated charcoal powder (Merck Specialities Pvt. Ltd., Mumbai) with poly methylmethacrylate (Alfa Aesar) in the weight ratio of 9:1. Here, acetone (Sigma Aldrich) was used as a solvent. The Torey carbon fibre paper (TGP-H-120, with bulk density of 0.45 g/cm^3 , electrical resistivity of $80 \text{ m}\Omega\text{cm}$ and thickness of 0.37 mm) served as the current collector and was coated with the carbon slurry. The coating was made with the help of a

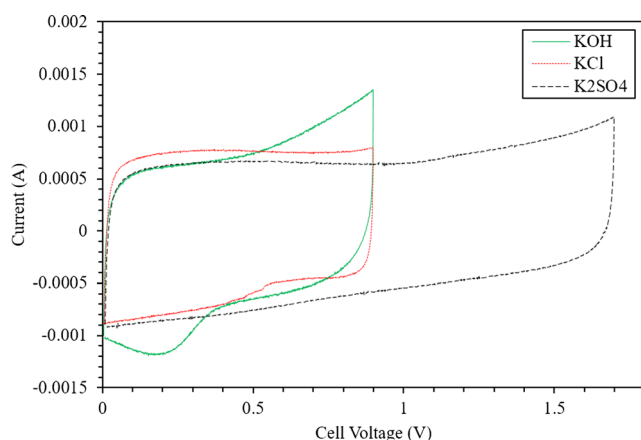


Fig. 2 Cyclic voltammograms for three electrolytes using symmetric two electrode cell

doctor's blade only on one side of the carbon fibre paper. The coated carbon papers were dried in an oven at $70 \text{ }^\circ\text{C}$ for 5 h. The thickness of the active layer was 0.07 mm . The size of the each electrode is $1 \text{ cm} \times 1 \text{ cm}$.

A symmetric EDLC cell was assembled in plexi glass with two identical electrodes, separated by Whatman® qualitative filter paper of grade 1. Aqueous solutions of 2 M KCl (Merck Specialities Pvt. Ltd., Mumbai), 0.5 M K_2SO_4 (Sigma Aldrich) and 6 M KOH (Merck Specialities Pvt. Ltd., Mumbai) were used as electrolytes in separate experiments. The concentrations were decided based on solubility and performance with other electrodes, as reported in literature. Experiments were also performed in three electrode cell, with Pt plate as the counter electrode and Ag/AgCl as the reference electrode. Cyclic Voltammetry, Electrochemical Impedance Spectroscopy and Galvanostatic Charge/Discharge experiments were performed using Versa STAT 3 potentiostat/galvanostat (Princeton Applied Research, USA). A voltage window of $0\text{--}0.9 \text{ V}$ was used for KOH and KCl electrolytes. In case of K_2SO_4 , $0\text{--}1.7 \text{ V}$ was taken as the voltage window for electrochemical analysis. The results from impedance spectroscopy were fitted to ladder-type equivalent circuit. Simplex algorithm was used for error minimization in Matlab R2013b from Mathworks Inc.

The Brunauer-Emmett-Teller (BET) surface area and pore size distribution of the carbon powder were estimated from nitrogen adsorption–desorption experiments (Autosorb 1 MP, Quantachrome Instruments, USA).

Results and discussions

Two most critical factors in the transport of electrolyte ions are the conductivity of the electrolyte and the pore structure of the electrode material. The adsorption–desorption experiment for

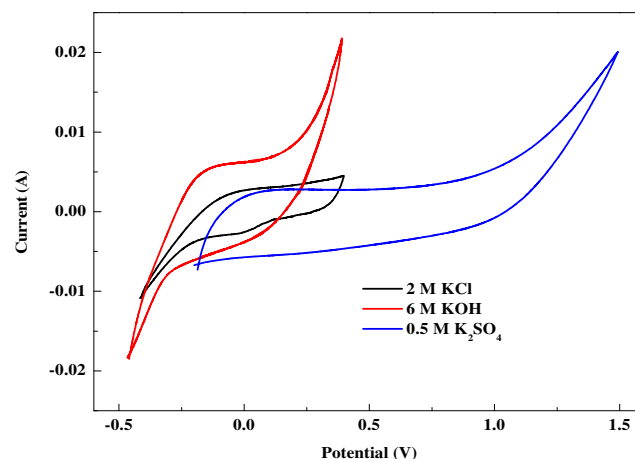


Fig. 3 Cyclic voltammograms for three electrolytes using three electrode cell

Table 1 Performance summary: specific capacitance of single electrode (C_s), energy density and coulombic efficiency

Electrolyte	Three electrode cell	Two electrode cell			
	C_s (F/g) (at 10 mV/s)	C_s (F/g) (at 10 mV/s)	C_s (F/g) (at 0.1 A/g)	Energy density (Wh/Kg)	Coulombic efficiency (%) (at 0.1 A/g)
KOH	73.10	71.7	66.8	3.76	97.28
KCl	32.32	59.3	62.1	3.49	94.25
K ₂ SO ₄	53.54	47.6	42.8	8.95	93.14

analysis of pore structure revealed the BET surface area of the carbon powder as 900.15 m²/g. The average pore radius and pore volume were found to be 1.16 nm and 0.49 cm³/g, respectively. After mixing with the binder, these values were reduced to 481.18 m²/g, 3.39 nm and 0.41 cm³/g, respectively. The pore size distribution from the density functional theory is given in Fig. 1. The presence of micro and meso pores is evident here. The micro pores are mostly in the size range of 0.3–1.5 nm. In order to achieve maximum capacitance, micro pores are the target sites for the double layer, as the micropores contain most of the internal surface area. The mesopores offer the rest of the internal surface. More importantly, the meso pores allow the transport of ions from the bulk electrolyte into the micro pores.

Cyclic Voltammetry (CV) curves are presented in Figs. 2 and 3. Specific capacitance is proportional to area inside the CV curve. This area represents the product of the average current and the applied voltage. Specific capacitance of single electrode in two and three electrode cell is estimated by the following equations: [28].

$$C_{\text{cell}} = \frac{\int_{V_1}^{V_2} I(V) dV}{2(V_2 - V_1)\vartheta} \text{ Cell capacitance} \quad (1)$$

$$C_{\text{electrode}} = 2 \times \frac{C_{\text{cell}}}{m} \text{ Specific capacitance in two electrode cell} \quad (2)$$

$$C_{\text{electrode}} = \frac{C_{\text{cell}}}{m} \text{ Specific capacitance in three electrode cell} \quad (3)$$

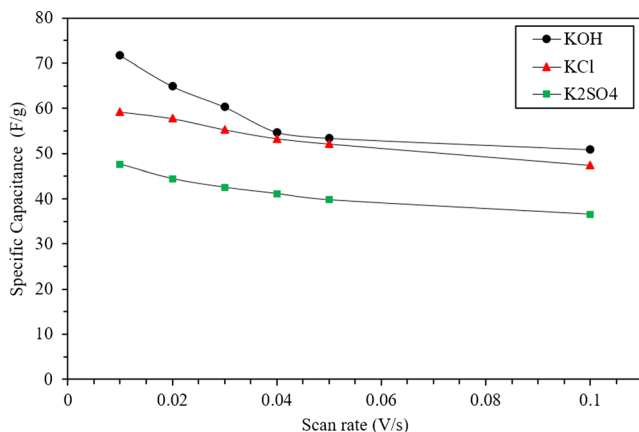


Fig. 4 Variation of specific capacitance with scan rate

Here $I(V)$ is the current, as a function of voltage V , $(V_2 - V_1)$ is the voltage window used, m is the mass of active electrode material for one electrode and ϑ is the scan rate. The specific capacitance values from the two electrode set-up are consistent with the results from the three electrode set-up (Table 1). In the case of three electrode set-up, a redox peak appeared at a lower voltage in the CV scan, compared to the results from the two electrode set-up. This is most possibly due to the oxygen functionality in activated charcoal. The highest specific capacitance was obtained, when KOH was the electrolyte. This is consistent with the high specific conductance of KOH. Also, for KOH as electrolyte, steep decrease in specific capacitance was observed, when the scan rate was increased from 10 to 100 mV/s (Fig. 4). Beyond this point, the specific capacitance remained unaltered with further increase in scan rate. The variation of the specific capacitance is not this significant in case of KCl and K₂SO₄ as the electrolytes. As such, lower scan rate allows the electrolyte ions to penetrate fully into the pore network and reaches an equilibrium in the formation of a double layer. Accordingly, a higher capacitance is expected at a lower scan rate. The ionic conductance of KOH is significantly higher in comparison with other two electrolytes and manifested in a larger change in capacitance with the scan rate. This may be noted here that the ionic conductivity of aqueous KOH, KCl and K₂SO₄ are 440, 208 and 120 mScm⁻¹ [15, 29, 30], respectively.

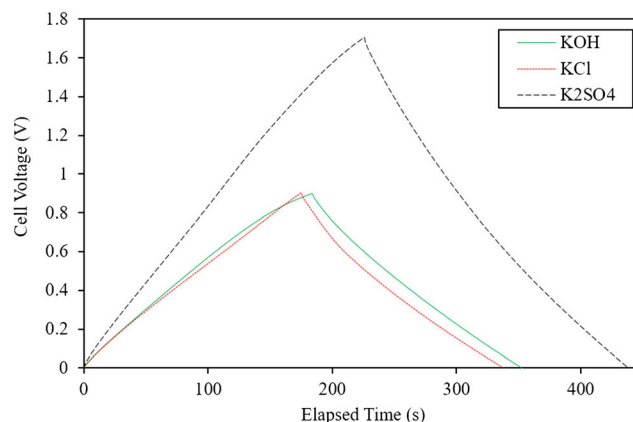


Fig. 5 Galvanostatic charge/discharge curves for three electrolytes

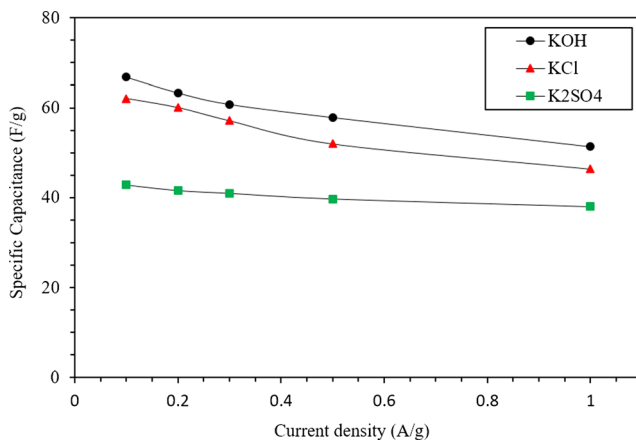


Fig. 6 Variation of specific capacitance with current density

The specific capacitance was also studied from galvanostatic charge–discharge experiments. The galvanostatic charge–discharge curves are presented in Fig. 5. Specific capacitance was calculated from galvanostatic charge and discharge data using the following equation: [28]

$$C_{\text{electrode}} = 2 \times C_{\text{cell}} = \frac{2 \times I}{\left(\frac{dV}{dt}\right)} \quad (4)$$

Here, I is the current density in A/g (mass of single electrode is taken); dV/dt is the slope of the discharge curve. The highest specific capacitance of 66.78 F/g was observed with KOH electrolyte at the current density of 0.1 A/g. The high value of specific capacitance for KOH is consistent with the results from cyclic voltammetry. As discussed earlier in the context of cyclic voltammetry results, the strong dependence of specific capacitance on charging rate for KOH electrolyte arises from higher ionic conductivity, smaller hydrated ion size and high ionic mobility. This is further discussed in latter sections of this article. The performances of the three electrolytes are summarized in Table 1. Variation of specific

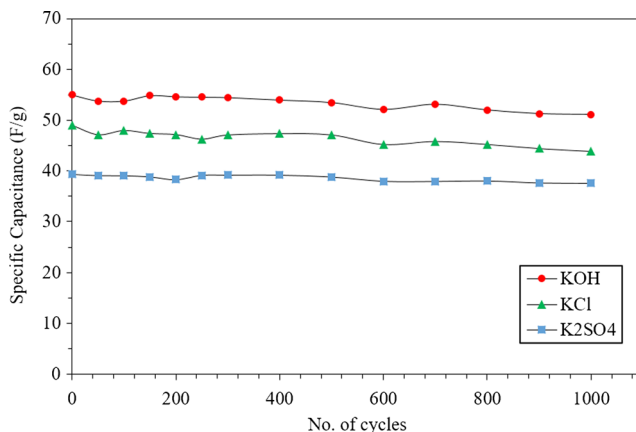


Fig. 7 Effect of charge–discharge cycles on the capacitance

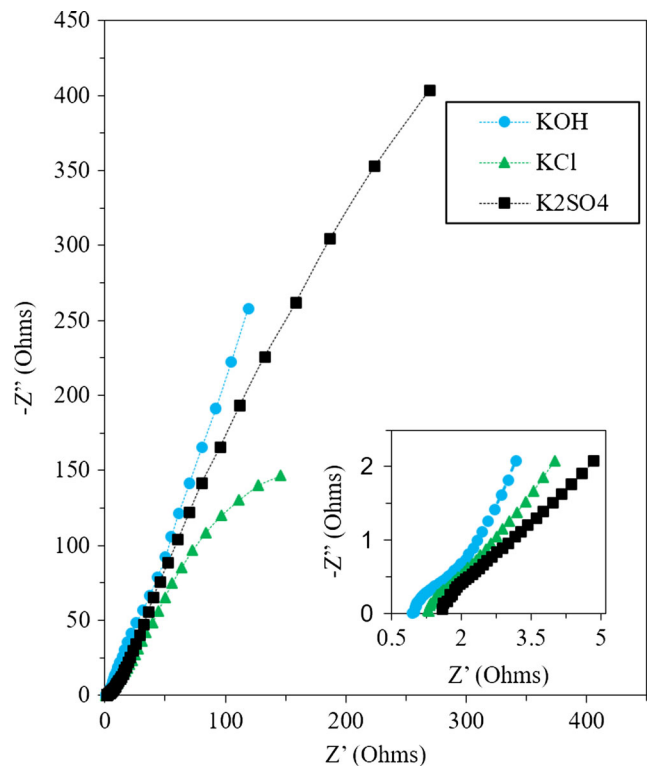


Fig. 8 Comparison of EIS data

capacitance with current density is plotted in Fig. 6. Significant drop in capacitance was observed with increase in current density from 0.1 to 1 A/g for KCl and KOH electrolytes. In case of K_2SO_4 electrolyte, the drop in capacitance is insignificant with change in current density from 0.1 to 1 A/g. Faster charging and discharging with uncompromised specific capacitance are evident, when K_2SO_4 was used as the electrolyte.

The stability with the three electrolytes was examined by submitting the EDLC to repeated charge–discharge cycles. The specific capacitance is plotted in Fig. 7 as a function of

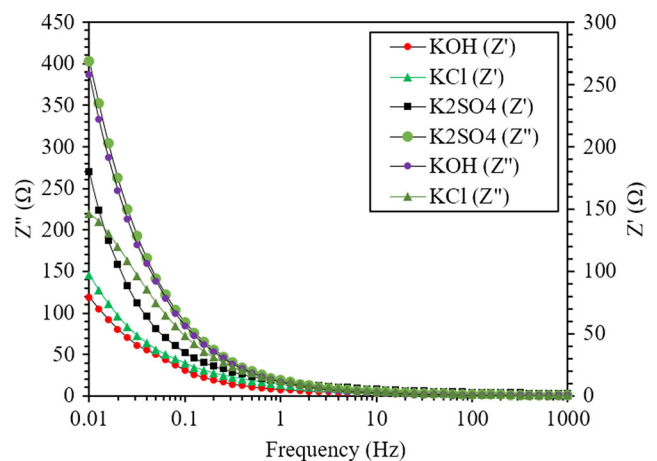


Fig. 9 Real and complex parts of impedance as a function of frequency for the three electrolytes

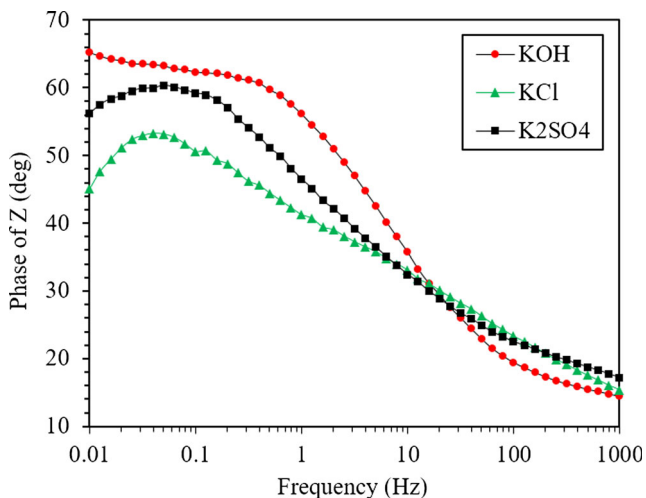


Fig. 10 Phase angle as a function of frequency for the three electrolytes

the number of charge–discharge cycles, performed prior to the measurement. After 1000 cycles, 96% of the specific capacitance was retained, with K₂SO₄ as the electrolyte. The retention with KCl and KOH electrolytes are 94 and 93%, respectively, after 1000 cycles.

The profile of an isosceles triangle for the charge–discharge cycle indicates an ideal behaviour, and allows the use of Eq. 5 to estimate the coulombic efficiency.

$$\eta_t = \left(t_c / t_D \right) \times 100 \tag{5}$$

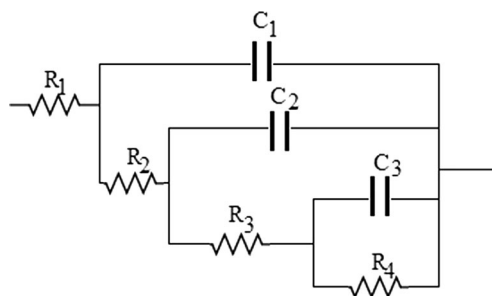


Fig. 12 Ladder-type equivalent circuit

Here, t_c is the time period for charging and t_D is the time period for discharging. The coulombic efficiency is another indicator of the stability of activated carbon electrodes with the three electrolytes. At the current density of 1 A/g, the coulombic efficiency was found to be 100% for all the three electrolytes. At a lower current density (0.1 A/g), the coulombic efficiency got slightly reduced to 97.28, 93.14 and 94.25% for KOH, KCl and K₂SO₄, respectively. The reduction at lower current density is possibly due to the side reactions from impurities, whose proportional contribution became insignificant at higher current densities. Further, the coulombic efficiency was estimated at the end of 100 cycles at the current density of 1 A/g. The efficiency was found 95 and 90%, respectively, for KOH and KCl as electrolyte. The efficiency remained 100%, when K₂SO₄ was the electrolyte.

With a consistent set of electrochemical responses involving the three electrolytes, further studies were undertaken to

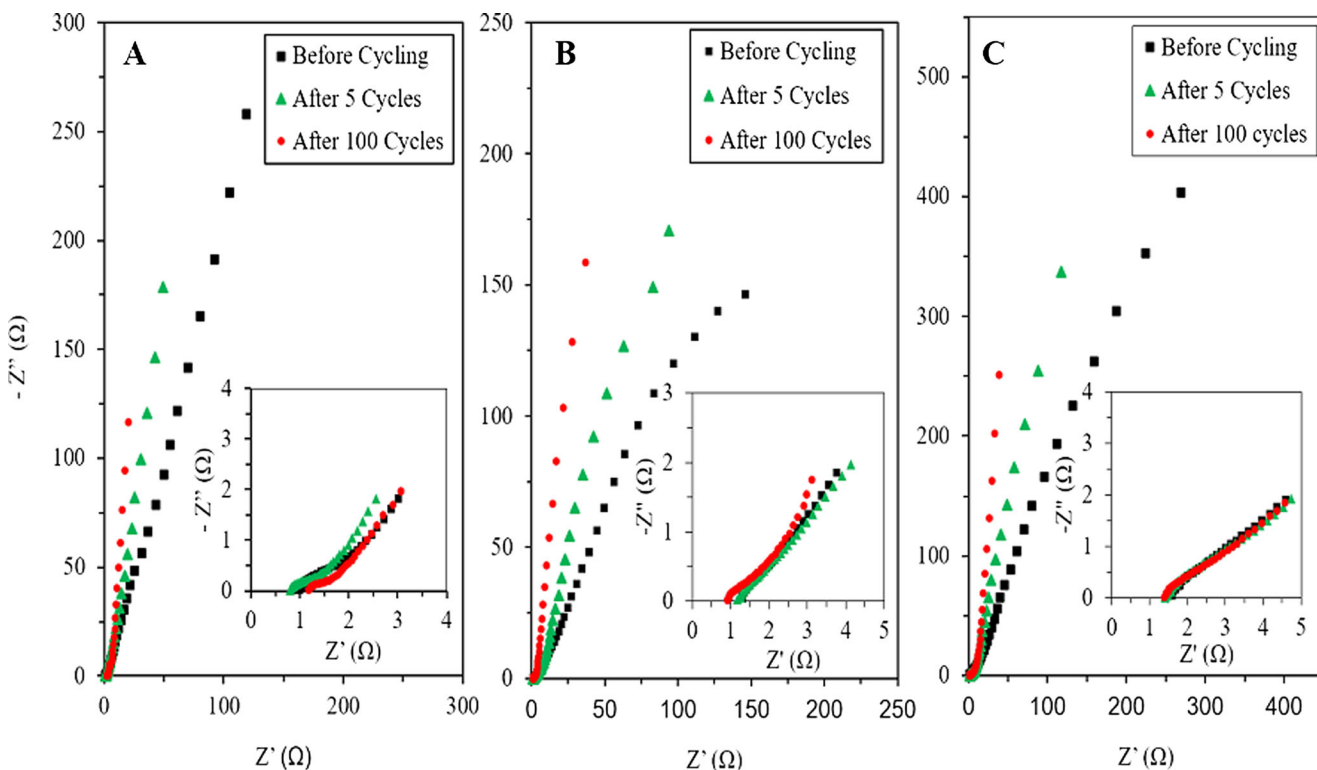


Fig. 11 Change in EIS profiles due to charge–discharge cycles for a KOH, b KCl and c K₂SO₄ electrolytes

Table 2 Regressed values of circuit parameters (κ is specific conductance of the electrolytes in mS/cm; R_1 is equivalent series resistance; C_1 is value of the capacitive element representing capacitance in first level pore hierarchy; C_2 and C_3 represents the capacitance for the intermediate and the lowest hierarchy pores, respectively; R_2 and R_3 are the resistances to charge propagation at intermediate and the lowest hierarchical pores)

Electrolyte	κ (mS/cm)	R_1 (Ω)	C_1 (F)	R_2 (Ω)	C_2 (F)	R_3 (Ω)	C_3 (F)	R_4 (Ω)	Chi ²
KOH	400	1.57	3.8×10^{-3}	6.81	0.011	61.36	0.017	223.1	0.082
KCl	208	2.11	1.4×10^{-3}	8.01	0.009	31.97	0.023	126.6	6.44×10^{-4}
K ₂ SO ₄	120	2.89	1.0×10^{-3}	11.02	0.007	66.25	0.011	348.5	0.119

analyse the characteristics of the double layer capacitance at varied extent of penetration by the electrolyte ions into the pore network. Electrochemical impedance spectroscopy (EIS) was performed in the frequency range of 0.01 Hz to 1 MHz. Nyquist plots for the three electrolytes are presented in Fig. 8. The same plot at higher frequency is shown in magnified form as inset of Fig. 8. EIS with KOH as electrolyte indicates the lowest value of equivalent series resistance (ESR = 0.97 Ω), when compared with the intercepts for KCl (1.3 Ω) and K₂SO₄ (1.55 Ω), respectively. ESR includes resistances offered by (i) electrode-electrolyte interface, (ii) electrode and current collector interface and (iii) bulk electrolyte resistance. The relative magnitudes of ESR for the three electrolytes are in agreement with the respective ionic conductivities. With regard to the bulk electrolyte resistance, the difference was made by the mobility of anions in the micropores. The cation (K⁺) remained same in all three electrolytes, though at different concentrations. The smaller hydrated ion size of the OH⁻ ions (0.4240 nm), higher ionic conductivity and a relative ionic mobility of 2.7 (relative to K⁺) resulted in the highest specific capacitance with KOH electrolyte. Small hydrated ion size of Cl⁻ (0.448 nm) and a relative ionic mobility of 1.03 (relative to K⁺) provided a moderate level of specific capacitance for the KCl electrolyte. The aqueous alkali sulphate showed the least specific capacitance due to larger hydrated anions (0.556 nm), lower ionic conductivity and low relative ionic mobility (0.54) [31–]. Table 4 presents the ESR values, reported in literature [33–35] for the given electrolytes. The ESR values are consistent with the values from the present study. Figs. 9 and 10 present the real and complex impedance, and the phase angle as a function of frequency. The phase angle varies from 90 to 45° with frequency as per the de Levi's model. The angle 90° refers to an ideal capacitor, and the 45° is derived from the transmission line model, describing transport of ion through a single uniform pore. In pore

network, with pore size distribution, the smaller pores are not penetrated, particularly when the frequency is large. Further, the penetration depends on the size of ions and the interaction with the internal surface. Hence, the net resistive and capacitive contributions, respectively, to the phase angle, varied with the type of electrolyte. This is reflected in the three different lines in Fig. 10.

One important aspect of this study is the longer-term electrode–electrolyte interactions and the stability of the electrode after several charge–discharge cycles. EIS was performed after 5 cycles and 100 cycles of charge–discharge, respectively. The effect of charge–discharge cycles on the Nyquist spectra is presented in Fig. 11. A nominal shift of Nyquist plot towards imaginary impedance axis was observed after the charge–discharge cycles, indicating some dynamic dispersion of ions inside the pores [14]. The magnitude of the shift was the highest in the case of KCl electrolyte. The ESR value, as observed from the intercept of the Nyquist plot to the real impedance axis was found to decrease slightly with the number of cycles.

The EIS data was further analysed through equivalent circuit model. The fitting of data to ladder-type electrical circuit is presented in Fig. 12. The circuit represents three levels of hierarchy in pore network. Here, one set of pores, branches into the other set. The parameter R1 includes the ESR. The parameters R2 and R3 represent the resistances to access pores at the lower level of hierarchy in the network. C3 represents the capacitance at the lowest hierarchy. The overall capacitance of the electrode will primarily be contributed from the pores at lower hierarchy (micro pores). R4 represents the leakage resistance associated with C3 and signifies the non-ideality in the double layer capacitance. Table 2 lists the converged values of circuit parameters. Table 2 indicates that the resistance outside the pore network (e.g., bulk electrolyte resistance) is the lowest for KOH. This is consistent with the

Table 3 Regressed values of circuit parameters after 5 cycles

Electrolyte	R_1 (Ω)	C_1 (F)	R_2 (Ω)	C_2 (F)	R_3 (Ω)	C_3 (F)	R_4 (Ω)	Chi ²
KOH	1.13	5.5×10^{-3}	2.17	0.027	19.85	0.031	143.3	0.034
KCl	1.77	1.7×10^{-3}	4.12	0.016	15.99	0.032	139.3	0.044
K ₂ SO ₄	2.21	8.3×10^{-4}	5.25	0.011	23.99	0.018	306.1	0.064

Table 4 The ESR values in literature for the given electrolytes in carbon electrodes

Electrode	Electrolyte	Specific capacitance	Equivalent series resistance
Activated carbon [33] obtained by heat treatment of bituminous at temperatures from 520 to 1000° C followed by KOH activation at 700 or 800° C	6 M KOH	286 F/g (0.1 A/g)	0.17 Ω
Nanoporous carbon black based [34]	2 M KCl	33.58 F/g (10 mV/s)	7.1 Ω.cm ²
Activated carbon from phenol-melamine-formaldehyde resin [35]	6 M KOH	210 F/g (2 mV/s)	1.33 Ω
Carbon powder based on activated charcoal	6 M KOH	71.7 F/g (10 mV/s) 66.8 F/g (0.1 A/g)	0.97 Ω
	2 M KCl	59.3 F/g (10 mV/s) 62.1 F/g (0.1 A/g)	1.3 Ω
	0.5 M K ₂ SO ₄	47.6 F/g (10 mV/s) 42.8 F/g (0.1 A/g)	1.55 Ω

intercept on the real axis in Fig. 8, as discussed before. However, at deeper levels of hierarchy, the resistances for KOH and K₂SO₄ become at par with each other. This shows the reduced importance of bulk electrolyte properties at the lowest level of hierarchy in the pore network. Further, the resistance to access the lowest hierarchy was the least, when KCl was the electrolyte. At the same time, the leakage resistance R₄ is the least for the KCl electrolyte. Therefore, the transport and charge storage at the lowest hierarchy shows some non-ideality with KCl that was not significant with other two electrolytes. After 100 cycles of charge–discharge, no major change in the fitted parameters was observed. The minor changes in the parameters may be attributed to the difference in mobility of ions. For example, SO₄²⁻ ions are much bulkier than OH⁻ and Cl⁻ ions, and their attachment to surface or penetration into the pores may not remain same after several charge–discharge cycles. The impurities at the surface, and side reactions, involving impurities may also change the values of the parameters to insignificant extent Tables 3 and 4.

The above analysis indicates KOH as the electrolyte of choice due to the ease of ion transport and the quality of the double layer. However, the highest energy density was observed with the K₂SO₄ electrolyte. The energy density is

directly proportional to the square of the charging voltage. The highest energy density for K₂SO₄ is because of the wide voltage window (0–1.7 V), within which no oxidation or reduction takes place. The Ragone plot for the three aqueous electrolytes is presented in Fig. 13. K₂SO₄ shows the highest energy density and power density and is suited for high power applications. The energy density and power density by K₂SO₄ electrolyte with activated carbon electrodes are 8.6 Wh/kg (at 0.1 A/g) and 6.2 kW/kg (at 1 A/g), respectively. KOH showed good power density, though lacked energy density to the level, realized by K₂SO₄.

Conclusions

The article addressed the transport of electrolyte ions and the quality of double layer capacitance in activated carbon electrodes with alkaline, neutral salt and alkali sulphate electrolytes, respectively. The trends with specific capacitance were found consistent with the ionic conductivity and hydrated anion size of the electrolytes. The results from cyclic voltammetry and chronopotentiometry show the highest specific capacitance with KOH as electrolyte that depends more strongly on the scan or charging rate. This behaviour is considered as another manifestation of the electrolyte's high ionic conductivity. The relative magnitudes of the equivalent series resistance from the EIS plots are consistent with the bulk ionic properties of the respective electrolytes. The EIS data was fitted to the ladder-type equivalent circuit. The converged values of resistance in the upper level of hierarchy are consistent with the ESR value and the ionic conductivity for the respective electrolytes. However, at lower level of pore hierarchy, the resistance to KOH electrolyte was found at par with the resistance to K₂SO₄ electrolyte. This is in contradiction to the respective ionic conductivities. Thus, the bulk electrolyte properties became less dominant at the level of micropores. Further, some non-ideality in transport and charge storage was observed with KCl electrolytes at the lowest hierarchy. After several cycles of charge–discharge, small changes in the EIS

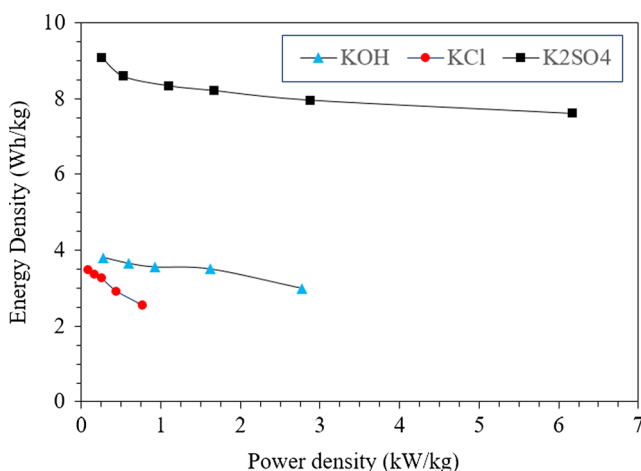


Fig. 13 Comparison of the performance of three electrolytes through Ragone plot

plots were observed, though the specific capacitance was retained to the extent of 96% after 1000 cycles. The importance of power and energy density is underscored through a comparison of the performances in Ragone plot.

References

- Conway BE (1999) *Electrochemical supercapacitors—scientific fundamentals and technological applications*. Kluwer Academic/Plenum Press, New York
- Kötz R, Carlen M (2000) Principles and applications of electrochemical capacitors. *Electrochim Acta* 45:2483–2498
- Sarangapani S, Tilak BV, Chen CP (1996) Materials for electrochemical capacitors: theoretical and experimental constraints. *J Electrochem Soc* 143:3791–3799
- Frackowiak E, Béguin F (2001) Carbon materials for the electrochemical storage of energy in capacitors. *Carbon* 39:937–950
- Kierzek K, Frackowiak E, Lota G, Gryglewicz G, Machnikowski J (2004) Electrochemical capacitors based on highly porous carbons prepared by KOH activation. *Electrochim Acta* 49(4):515–523
- Qu D, Shi H (1998) Studies of activated carbons used in double-layer capacitors. *J Power Sources* 74:99–107
- Guo Y, Qi J, Jiang Y, Yang S, Wang Z, Xu H (2003) Performance of electrical double layer capacitors with porous carbons derived from rice husk. *Mat Chem Phys* 80:704–709
- Bleda-Martínez MJ, Maciá-Aguló JA, Lozano-Castelló D, Morallón E, Cazorla-Amorós D, Linares-Solano A (2005) Role of surface chemistry on electric double layer capacitance of carbon materials. *Carbon* 43(13):2677–2684
- Kim YJ, Horie Y, Matsuzawa Y, Ozaki S, Endo M, Dresselhaus MS (2004) Structural features necessary to obtain a high specific capacitance in electric double layer capacitors. *Carbon* 42:2423–2432
- Shiraishi S, Kurihara H, Tsubota H, Oya A, Soneda Y, Yamada Y (2001a) Electric double layer capacitance of highly porous carbon derived from lithium metal and polytetrafluoroethylene. *Electrochem Solid State Lett* 4:A5–A8
- Lozano-Castelló D, Cazorla-Amorós D, Linares-Solano A, Shiraishi S, Kurihara H, Oya A (2003) Influence of pore structure and surface chemistry on electric double layer capacitance in non-aqueous electrolyte. *Carbon* 41:1765–1775
- Shi H (1996) Activated carbons and double layer capacitance. *Electrochim Acta* 41:1633–1639
- Waidhas M, Mund K (1996) In: Delnick FM, Ingersoll D, Andrieu X, Naoi K (eds) *Proceedings of the symposium on electrochemical capacitor II*. The Electrochemical Society, Pennington, p 180
- Qu QT, Wang B, Yang LC, Shi Y, Tian S, Wu YP (2008) Study of electrochemical performance of activated carbon in aqueous Li_2SO_4 , Na_2SO_4 and K_2SO_4 electrolytes. *Electrochem Commun* 10:1652–1655
- Salitra G, Soffer A, Eliad L, Cohen Y, Aurbach D (2000) Carbon electrodes for double-layer capacitors I. Relations between ion and pore dimensions. *J Electrochem Soc* 147(7):2486–2493
- Shiraishi S, Kurihara H, Oya A (2001b) Electric double layer capacitance of mesoporous activated carbon fiber. *Electrochemistry* 69:440–443
- Gryglewicz G, Machnikowski J, Lorenc-Grabowska E, Lota G, Frackowiak E (2005) Effect of pore size distribution of coal-based activated carbons on double layer capacitance. *Electrochim Acta* 50:1197–1206
- Lin C, Ritter JA, Popov BN (1999) Correlation of double-layer capacitance with the pore structure of Sol-gel derived carbon Xerogels. *J Electrochem Soc* 146:3639–3643
- Keiser H, Beccu KD, Gutjahr MA (1976) Abschätzung der porenstrukturporöserelektrodenausimpedanzmessungen. *Electrochim Acta* 21:539–543
- Candy JP, Fouilloux P, Keddad M, Takenouti H (1981) The characterization of porous electrodes by impedance measurements. *Electrochim Acta* 26:1029–1034
- Taberna PL, Simon P, Fauvarque JF (2003) Electrochemical characteristics and impedance spectroscopy studies of carbon-carbon supercapacitors. *J Electrochem Soc* 150(3):A292–A300
- Lufrano F, Staiti P, Minutoli M (2003) Evaluation of nafion based double layer capacitors by electrochemical impedance spectroscopy. *J Power Sources* 124:314–320
- Jang JH, Oh SM (2004) Complex capacitance analysis of porous carbon electrodes for electric double-layer capacitors. *J Electrochem Soc* 151:A571
- Srinivasan V, Weidner JW (1999) Mathematical modeling of electrochemical capacitors. *J Electrochem Soc* 146(5):1650–1658
- Yoon S, Jang JH, Ka BH, Oh SM (2005) Complex capacitance analysis on rate capability of electric-double layer capacitor (EDLC) electrodes of different thickness. *Electrochim Acta* 50:2255–2262
- Jang JH, Yoo S, Ka BH, Oh SM (2005) Complex capacitance analysis on leakage current appearing in electric double-layer capacitor carbon electrode. *J Electrochem Soc* 152:A1418–A1422
- Honda K, Rao TN, Tryk DA, Fujishima A, Watanabe M, Yasui K, Masuda H (2001) Impedance characteristics of the nanoporous honeycomb diamond electrodes for electrical double-layer capacitor applications. *J Electrochem Soc* 148:A668–A679
- Yu D, Qian Q, Wei L, Jiang W, Goh K, Wei J, Zhang J, Chen Y (2015) Emergence of fibre supercapacitors. *Chem Soc Rev* 44:647–662
- Weast RC (1989) *CRC handbook of chemistry and physics*, 70th edn. CRC Press, FL, p D-221
- Wolf AV (1966) *Aqueous solutions and bodily fluids*. Harper and Row, New York
- Hasegawa G, Kanamori K, Nakanishi K, Abe T (2012) New insights into the relationship between micropore properties, ionic sizes, and electric double-layer capacitance in monolithic carbon electrodes. *J Phys Chem C* 116(50):26197–26203
- Dean JA (1999) *Lange's handbook of chemistry*, 15th edn. McGraw-Hill, New York
- Raymundo-Pinero E, Kierzek K, Machnikowski J, Béguin F (2006) Relationship between the nanoporous texture of activated carbons and their capacitance properties in different electrolytes. *Carbon* 44:2498–2507
- Nasibi M, Golozar MA, Rashed G (2003) Nanoporous carbon particles as an electrode material for electrochemical double layer supercapacitors. *Material Letters* 91:323–325
- Shen H, Liu E, Xiang X, Huang Z, Tian Y, Wu Y, Wu Z, Xie H (2012) A novel activated carbon for supercapacitors. *Mater Res Bull* 47:662–666